Pergamon

*Electrochimica Acta,* Vol. 43, Nos 19–20, pp. 2875–2888, 1998
© 1998 Published by Elsevier Science Ltd. All rights reserved
Printed in Great Britain
PII: S0013-4686(98)00028-0
0013–4686/98 $19.00 + 0.00

# Ionic adsorption at the Au(111) electrode

Jacek Lipkowski,[a]* Zhichao Shi,[a] Aicheng Chen,[a] Bruno Pettinger[b] and Christoph Bilger[b]

[a]Department of Chemistry and Biochemistry, University of Guelph, Guelph, Ont., Canada N1G 2W1

[b]Fritz-Haber-Institute der Max-Planck-Gesellshaft, Department of Physical Chemistry, Faradayweg 4–6, D-14195 Berlin, Germany

(Received in Newcastle 21 January 1998)

**Abstract**—This paper reviews thermodynamic, spectroscopic and X-ray diffraction studies of $SO_4^{2-}$, $Cl^-$, $Br^-$ and $I^-$ adsorption at the Au(111) electrode surface. The thermodynamic experiments provided information about surface concentrations of specifically adsorbed anions, Gibbs energies of adsorption and the numbers of unit charge flowing to the interface per one adsorbed anion. Second harmonic generation and surface X-ray scattering revealed the affect of ionic adsorption on the electronic and crystallographic structure of the interface. The atomistic information derived from these microscopic studies was used to discuss the thermodynamic data and to verify the theoretical models of the interface. It has been shown that complete description of ionic adsorption at metal electrodes requires a concerted use of the macroscopic and microscopic techniques. © 1998 Published by Elsevier Science Ltd. All rights reserved

*Key words:* ionic adsorption, gold electrode, double layer structure.

## INTRODUCTION

Most of our past knowledge concerning ionic adsorption came from thermodynamic studies at mercury electrodes [1]. For long the thermodynamic measurements performed with solid electrodes have been much less accurate and were plagued by problems related to the surface cleanliness and reproducibility of the surface morphology. However, ionic adsorption at solid electrodes may be investigated not only by thermodynamic methods but also by numerous spectroscopic, diffraction and surface imaging techniques. The information gained from thermodynamic measurements may be enriched by a complementary structural information. The interest in studies of ionic adsorption on solid electrodes is therefore significant.

Among the solid metals, gold has unique properties as electrode material. The range of potentials where it displays ideal or nearly ideal polarizable behavior exceeds 1 V. Hence, the adsorption processes may be investigated over the range of surface charge densities that spans almost 100 $\mu C\,cm^{-2}$. For other metals, the metal dissolution and hydrogen adsorption–evolution processes restrict this range of potentials and charges significantly. The development of the flame annealing treatment of noble metal electrodes provided a simple and reliable method to clean gold surfaces and to reproducibly restore their surface crystallography [2]. Consequently, the thermodynamic data measured for gold electrodes, particularly those determined by the chronocoulometric technique [3], are nearly as precise as for mercury. Finally, gold is an ideal electrode material for spectroscopic, diffraction and surface imaging studies of interfacial processes [4]. For all these reasons, ionic adsorption at gold electrodes has been recently investigated by many macroscopic and microscopic techniques. The most extensive studies were performed for the Au(111) surface. Sulfate adsorption at the Au(111) electrode was investigated by chronocoulometry and radiochemistry [5, 6], second harmonic generation (SHG) spectroscopy [7], cyclic voltammetry [8–10], LEED and photoelectron spectroscopies [11–14], STM [4, 15–17], IR spectroscopy [16, 17] and the

*Author to whom correspondence should be addressed.

electrochemical quartz crystal microbalance (EQCM) technique [18]. Chloride adsorption was studied by chronocoulometry [19] and radiochemistry [20], cyclic voltammetry [8], surface X-ray scattering [21] and EQCM [22]. Bromide adsorption at Au(111) surface was investigated by chronocoulometry [23], XPS and LEED [24, 25], SHG [26–29], STM [4, 30], SXS [21, 31–33], electroreflectance spectroscopy [34, 35] and EQCM [22, 36]. Finally, iodide adsorption at Au(111) surface was probed by LEED and electron spectroscopies [37, 38], STM [30, 39–44], SXS [45] and EQCM [22].

The purpose of this paper is to integrate the results of the thermodynamic (macroscopic) and structural (microscopic) studies into a unified picture of ionic adsorption at gold surfaces. We would like to demonstrate that a complete description of ionic adsorption at a metal electrode requires a concerted use of these two classes of techniques. We will use the example of adsorption of three halides ($I^-$, $Br^-$ and $Cl^-$) and will contrast the surface behavior of these simple ions to the properties of a polyatomic oxy-anion such as sulfate. The material presented in this paper is restricted to the case of the Au(111) electrode since studies of ionic adsorption at other crystallographic orientations of gold are incomplete.

## EXPERIMENTAL

The chronocoulometric technique was used to study energetics of ionic adsorption [3, 46]. The specific adsorption of ions was always investigated in the presence of a large excess of an inert electrolyte (0.1 M $KClO_4$). Therefore, the adsorption took place from mixed electrolyte solutions of a constant ionic strength. The thermodynamic parameters were calculated from the charge density data using the procedure described in [5]. The second harmonic generation spectra were acquired using YAG laser pulses of ca. 5 ns pulse with 100 mJ energy with a repetition of 5 Hz and photon wavelength of 1064 nm (photon energy 1.17 eV). Details of the SHG experiments are given in [7, 26–29]. The SHG data reported here were obtained using the interference SHG method [26]. In this technique, a quartz lamella is placed into the fundamental beam at two different positions, $x_1$ and $x_2$. The ISHG experiment requires recording the intensities of second harmonics photons for three experimental configurations, one without the quartz lamella ($I^{SHG}$) and two with the quartz lamella at either locations $x_1$ or $x_2$, ($I^{ISHG}(x_1)$, $I^{ISHG}(x_2)$). From these measured intensities, one can subsequently calculate the phase shift between the SHG signal generated at the electrode surface and the SHG signal generated by the quartz lamella at position $x_1$ [26].

## RESULTS AND DISCUSSION

### Energetics

The energetics of sulfate and halides adsorption at the Au(111) surface have been recently described for $SO_4^{2-}$, $Cl^-$, $Br^-$ and $I^-$ in Refs. [5, 6], [19], [23] and [47], respectively. The main results of these studies are summarized in Fig. 1. The top panel shows the cyclic voltammetry curves (CVs) recorded for millimolar concentrations of sulfate, chloride, bromide and iodide. The CVs recorded in the presence of the four anions display very similar shapes. These results are consistent with CVs published earlier in the literature [2, 48, 49]. Starting from the negative end and moving in the positive direction, each curve is characterized by a tall peak followed by a broad peak and a small reversible peak near the positive limit of potentials.

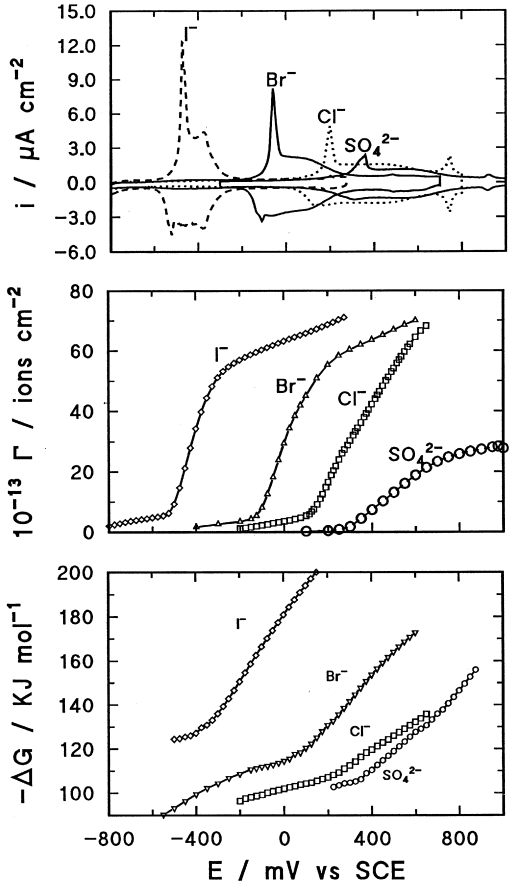


Fig. 1. Comparison of $SO_4^{2-}$, $Cl^-$, $Br^-$ and $I^-$ adsorption at the Au(111) electrode surface from 0.1 M $HClO_4 + 10^{-3}$ M $K_2SO_4$ and 0.1 M $KClO_4 + 10^{-3}$ M KCl, KBr and KI solutions. Top panel, cyclic voltammograms at a sweep rate of 10 mV $s^{-1}$. Middle panel, Gibbs excess vs. potential plots. Bottom panel, Gibbs enegry of adsorption. Standard state is an "ideal" $\Gamma$ = 1 ion $cm^{-2}$ for the surface species and an "ideal" $c$ = 1 mol $dm^{-3}$ for the bulk species

Recent surface X-ray diffraction [21–33, 45] and STM [4, 15, 16, 30, 37, 39] experiments indicate that the tall peak corresponds to the lifting of the reconstruction of the Au(111) surface. The Au(111) surface is reconstructed at potentials negative to this peak and has $(p \times \sqrt{3})$ structure. The reconstruction is lifted at potentials positive to the peak, where the surface has $(1 \times 1)$ structure. The tall peak is asymmetric and this asymmetry indicates that the kinetics of the lifting or restoring of the reconstructed surface are slow [31]. The position of the tall peak coincides also with the potential of zero charge for a given electrolyte [48]. The metal surface is negatively charged at potentials negative to this peak and positively charged at potentials which are more positive. The broad peaks correspond to the region of higher coverages where the adsorbed anions are mobile and the small reversible peaks at the positive end of potentials mark the formation of an ordered overlayer of adsorbed anions.

The middle panel in Fig. 1 shows changes of the surface concentration (Gibbs excess) of the four anions with the electrode potential. The adsorption of anions starts at a negatively charged surface, that is at potentials a few hundred millivolts more negative than the potential of the tall peak. Initially, the surface concentration of the anion changes slowly with potential so that a long foot is seen on the $\Gamma$ vs. $E$ plot. The surface concentration rises steeply at potentials corresponding to the position of the tall peaks on the cyclic voltammetry curves. At more positive potentials the surface concentration of anions attains a quasi plateau. It is useful to compare the measured maximum surface concentrations to the packing densities corresponding to the closed packed hexagonal monolayer of the four anions. The latter may be estimated using Van der Waals radii for halides [50] and the dimensions of $SO_4^{2-}$ taken from [51]. The calculated packing densities amount to $6.3 \times 10^{14}$ ions cm$^{-2}$ for iodide, $8 \times 10^{14}$ ions cm$^{-2}$ for bromide, $9 \times 10^{14}$ ions cm$^{-2}$ for chloride and $6.6 \times 10^{14}$ ions cm$^{-2}$ for sulfate. For halides, the maximum surface concentrations observed at the positive end of potentials agree within a few percent with the packing densities estimated from the Van der Walls radii. For comparison, the maximum surface concentration of halides measured at mercury amounted to only 30% of the maximum packing density [52]. Clearly, gold electrodes provide a unique opportunity to study halides adsorption in the whole range of surface concentrations. In contrast to halides, the maximum packing density measured for sulfate is only about one third of the calculated value. This result indicates that adsorption of sulfate and halide ions has somewhat different character. Within the plateau region, the surface concentrations of anion vary smoothly and do not display discontinuities at potentials where small reversible peaks are seen on CVs. This behavior indicates that the transition from disordered to ordered state of the adlayer proceeds without any significant change of the surface concentration of anions. The formation of the ordered adlayer is observed at surface concentrations that are very close to the saturation value.

The bottom panel in Fig. 1 shows the Gibbs energy plots. These data demonstrate that the strength of ionic adsorption increases by moving from sulfate to iodide. The Gibbs energy plots are nonlinear and may be seen as composed of two or three segments. This nonlinearity is consistent with the multiple state character of ionic adsorption seen also as the multiplicity of peaks on the cyclic voltammetry curves. The derivative of the Gibbs energy with respect to potential gives the charge number per adsorbed anion. The nonlinearity of Gibbs energy curves indicates that the charge number changes with potential or/and with the change of the adsorbed state. This point will be discussed in detail below.

## Charge numbers

Cross differentiation of the electrocapillary equation gives two charge numbers (numbers of unit charge flowing to the electrode per one adsorbed anion) [53]:

$$\gamma' = -\frac{1}{F}\left(\frac{\partial \sigma_M}{\partial \Gamma}\right)_E = \frac{1}{F}\left(\frac{\partial \mu}{\partial E}\right)_\Gamma \qquad (1)$$

and

$$n' = -\frac{1}{F}\left(\frac{\partial \sigma_M}{\partial \Gamma}\right)_\mu = \frac{1}{F}\left(\frac{\partial \mu}{\partial E}\right)_{\sigma_M} \qquad (2)$$

where $\gamma'$: is the charge number at a constant electrode potential and is usually known as electrosorption valency (IUPAC recommends symbol $l$ and the name "formal partial charge number" [53]) and $n'$: the charge number at a constant chemical potential

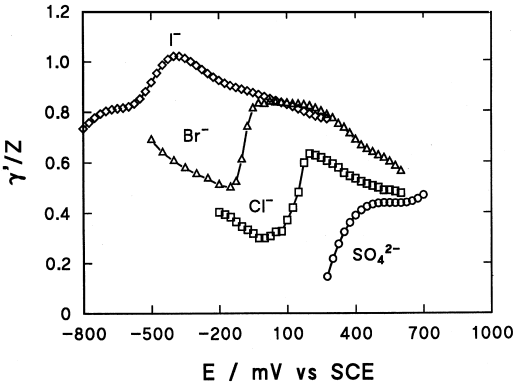


Fig. 2. Electrosorption valencies determined from the plots of the charge vs. the Gibbs excess at constant potential for $SO_4^{2-}$, $Cl^-$, $Br^-$ and $I^-$ adsorption at the Au(111) electrode surface

is equal to the reciprocal of the Esin–Markov coefficient.

Figure 2 shows how the electrosorption valency determined for the four anions changes with potential. To facilitate the comparison, the electrosorption valencies were divided by $z$, the charge of the anion with $z = -1$ for halides and $z = -2$ for sulfate. The electrosorption valency plots display a sigmoidal shape. For $Br^-$ and $Cl^-$, and $SO_4^{2-}$ the curves may be seen as composed of two segments with negative slopes separated by a step. The first segment, at more negative potentials, corresponds to adsorption of anions at the negatively charged surface while the second segment corresponds to adsorption at the positively charged electrode. The step is observed at the potential of zero charge. Apparently, $\gamma'/z$ increases when the charge at the metal surface changes sign. For iodide, the $\gamma'/z$ plot displays features similar to that observed for the two other halides, with the distinction that the segment corresponding to adsorption at the negatively charged surface has a different slope.

In contrast to the strong dependence of the electrosorption valency on potential, the Esin–Markov coefficient (which is the reciprocal of the charge number at a constant chemical potential) depends only weakly on charge. This point is illustrated by Fig. 3, where the surface concentrations of anions are plotted against the charge density at the metal, for $5 \times 10^{-3}$ M solutions of the four anions. The $\Gamma$ vs. $\sigma_M$ plots are fairly linear in the whole range of positive charge densities and, in this range, their slopes give singular values of the charge numbers at constant chemical potential. In electrons per one adsorbed anion, these numbers are $-1.4$ for $SO_4^{2-}$ [6]; $-0.95$ for $Cl^-$ [19], $-0.97$ for $Br^-$ [23] and $-0.96$ for $I^-$ [47]. The charge numbers at constant chemical potential depend only weakly on the bulk concentration of the anion. However, in Fig. 3, for halides, the experimental points corresponding to the region of negative charge densities, deviate systematically from the linear dependence. In this range, the charge number $n'$ amounts to about $-1.5$. The differences between the magnitude of charge numbers at constant electrode potential and at constant chemical potential are substantial. Due to these differences significant errors may result if these two charge numbers are confused. In fact, while electrosorption valency is frequently used in electrochemical literature, references to the charge number at constant chemical potential (Esin–Markov coefficient) are much less common. To make things worse, in a few cases these two charge numbers were confused. Below, we will discuss how electrosorption valencies and reciprocals of the Esin–Markov coefficients should be used to calculate surface coverages from integrated cyclic voltammograms.

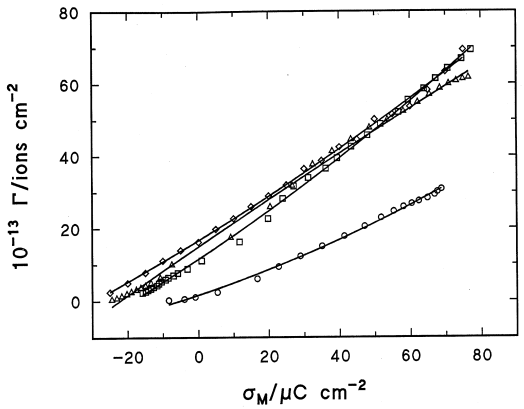


Fig. 3. Plots of the Gibbs excess against the electrode charge density for 0.1 M $HClO_4 + 5 \times 10^{-3}$ M $K_2SO_4$ (○) and 0.1 M $KClO_4 + 10^{-3}$ M KCl (□), KBr (△) and KI (◇) solutions

### How to use charge numbers

Surface coverages of an adsorbed ion are frequently calculated by integration of the cyclic voltammogram. Taking into account that the voltammetric current is equal to the product of the sweep rate $v$ and the differential capacity $C$, the integral of the voltammetric curve is equal to:

$$\Delta\sigma_M = \int i\,dt = \frac{1}{v}\int i\,dE = \int C\,dE \qquad (3)$$

The electrosorption valency, or the reciprocal of the Esin–Markov coefficient, have to be used to calculate the coverage of anion from the charge $\Delta\sigma_M$.

If the electrosorption valency is used to calculate $\Gamma$, the following procedure should be followed. In the presence of a specific adsorption of an anion, the capacity $C$ is a sum of two terms; the so called infinite frequency capacity $C_\Gamma$ and a pseudo-capacity $\gamma' F(d\Gamma/dE)$.

$$C = C_\Gamma + \gamma' F\frac{d\Gamma}{dE} \qquad (4)$$

By substituting $C$ in equation (3) by the right hand side of equation (4), the expression for $\Delta\sigma_M$ may be written as:

$$\Delta\sigma_M = \int C\,dE = \int C_\Gamma\,dE + \int \gamma'\,d\Gamma \qquad (5)$$

If the integration starts at a potential at which $\Gamma = 0$ and the electrosorption valency is independent of the electrode potential and coverage the result is:

$$\Delta\sigma_M = \int C_\Gamma\,dE + \gamma' F\Gamma \qquad (6)$$

equation (6) shows that the charge measured by integration of the cyclic voltammogram is a sum of $\gamma' F\Gamma$ and a term which corresponds to charging the infinite frequency capacity. In order to calculate $\Gamma$,

the integral has to be corrected for the $\int C_\Gamma \, dE$ term. Since different approximations are used to estimate the magnitude of $\int C_\Gamma \, dE$, this correction may introduce significant error to the calculated coverages [54–57]. In addition, as the data presented in Fig. 2 shows, the electrosorption valency may vary quite significantly with potential. In such a case, equation (6) should not be used to calculate the coverage.

It is much easier to use the reciprocal of the Esin–Markov coefficient to calculate the coverage from the integrated voltammogram. If the integration starts at the potential corresponding to the onset of adsorption, with the help of equation (2), the charge $\Delta\sigma_M$ may be expressed as equal to:

$$\Delta\sigma_M = -\int_0^\Gamma \left(\frac{\partial\sigma_M}{\partial\Gamma}\right)_\mu d\Gamma = -\int_0^\Gamma Fn' \, d\Gamma \qquad (7)$$

and if $n'$ is independent of $\Gamma$, the charge may be expressed as:

$$\Delta\sigma_M = n'FT \qquad (8)$$

equation (8) may be used to calculate surface concentrations provided $n'$ is known.

However, the Esin–Markov coefficients are seldom measured and these data are often not available. Occasionally, the electrosorption valency is incorrectly used in equation (8) instead of the reciprocal of the Esin–Markov coefficient. For example, for the Au(111) electrode, Uchida *et al.* [18] used equation (8) to calculate surface concentrations of sulfate from the integrated cyclic voltammograms. They incorrectly used the electrosorption valency instead of the reciprocal of the Esin–Markov coefficient. In addition, they assumed that $\gamma'$ is equal to $-1$ while the experimental value of the reciprocal of Esin–Markov coefficient is $-1.4$. Their results are about 30% higher than the coverages determined by chronocoulometry and radiochemistry [5]. Would they have used the reciprocal of the Esin–Markov coefficient, they would obtain surface coverages in a reasonable agreement with the chronocoulometric and radiochemical measurements. Indeed, in the most recent paper [22], they correctly used the Esin–Markov coefficient to calculate surface coverages for halides and their results were in good agreement with the chronocoulometric data. This example shows the limitation of the method based on the integration of the cyclic voltammetry curves. The method works provided the charge numbers at a constant chemical potential are known. Since the data concerning the Esin–Markov coefficients are scarce, the charge numbers have to be frequently estimated which may lead to a significant experimental error.

### Polarity of the surface bond

The electrosorption valency is frequently interpreted as a partial charge transfer coefficient. Within this concept, a stepwise increase of the electrosorption valency, such as that observed in Fig. 2, may be interpreted in terms of a progressive discharge of the adsorbed anion and formation of a halogen adatom. At this point, it is useful to recall that the electrosorption valency is a thermodynamic quantity, which is determined using Gibbs thermodynamics and hence Gibbs model of the interface. The model assumes that the interface is a two-dimensional dividing plane located somewhere between the two neighboring phases. The location of the interface is not known exactly and therefore we do not know to what location the $\gamma'$ charges flow when one anion is adsorbed. The charge number $\gamma'$ may equally well represent a total or a partial discharge of the adsorbed anion or may simply indicate that $\gamma'$ electrons flow out from surface so that the surface acquires a positive charge needed to screen the negative charge of the adsorbed anion. This second interpretation assumes a total separation of charge between the metal and the adsorbed anion. In that case the electrosorption valency may be interpreted as a thickness ratio:

$$\gamma'/z = (x_2 - x_1)/x_2 \qquad (9)$$

as discussed by Grahame [52] and Grahame and Parsons [58], where $x_2$ and $x_1$ are the distances of the outer and the inner Helmholtz planes from the metal surface respectively. Within this model, a change of the electrosorption valency is interpreted in terms of a change of the inner layer distance. Specifically, an increase of $\gamma'/z$ by moving from negatively charged to positively charged surface indicates that the distance between the adsorbed anion and the surface decreases, or in other words, that the electrosorption bond becomes shorter. This is a realistic interpretation since the electrosorption bond is expected to be shorter at the positively charged surface, due to the contraction of the electronic wave functions (contraction of the spill-over of electrons) and to the more efficient screening of the anion by the charge on the metal. However, this interpretation also deviates from the Gibbs model since it assumes a specific location for the adsorbed species (inner Helmholtz plane).

In reality, thermodynamic quantities provide little information about charge distribution at the interface and their interpretation requires a physical model whose validity cannot be proven on the basis of electrochemical measurement alone. In these circumstances it is much better to discuss the changes of the electrosorption valency in terms of the surface dipole ($\mu_s$) which represents a dipole formed by an adsorbed anion and its image charge in the metal. Parsons and co-workers [59, 60] and later Schmickler and Guidelli [61–66] have demonstrated that the dipole moment may be calculated from the electrosorption valency with the help of the formula:

$$\mu_s = \frac{(ze_0\varepsilon(1-\gamma'/z)}{{}_\sigma C} \qquad (10)$$

where $e_0$ is the unit charge, $\varepsilon$ is the permittivity and ${}_\sigma C$ is the capacity of the inner layer at the constant amount of adsorbed anion. The advantage of this approach is that the magnitude of the surface dipole is a direct measure of the polarity of the bond formed between the adsorbed anion and the metal. The dipole moment is given by product of the charge on adsorbed anion and the distance from its image charge in the metal. As in any other area of physical chemistry, the knowledge of the magnitude of the dipole moment is sufficient to describe the character of the electrosorption bond. There is no need to speculate about the magnitude of the charge on the adsorbed anion and the electrosorption bond length, when these quantities cannot be directly measured.

The dipole moments calculated for sulfate, chloride and bromide at the Au(111) surface are plotted against the charge on the metal in Fig. 4. The permittivity was taken as equal to the permittivity of vacuum ($\varepsilon_0 = 8.85 \times 10^{-12}$ C$^2$ J$^{-1}$ m$^{-1}$) in these calculations. The dipole moments for adsorbed anions have negative sign, however, in the following we will discuss their absolute values only. Overall, the values of the dipole moment increase in the order $Br^- < Cl^- < SO_4^{2-}$ indicating that the polarity of the dipole moment increases by moving from $Br^-$ to $SO_4^{2-}$. Apparently, the polarity of the electrosorption bond is a strong function of the charge on the metal. For adsorbed $Br^-$ and $Cl^-$, the polarity is large at the negatively charged surface, but decreases significantly at positive charges. In contrast, for adsorbed $SO_4^{2-}$ the polarity of the bond becomes quite large at positive charges. These results indicate that there are significant differences between the adsorption behavior of simple halide ions and this polyatomic oxy-anion.

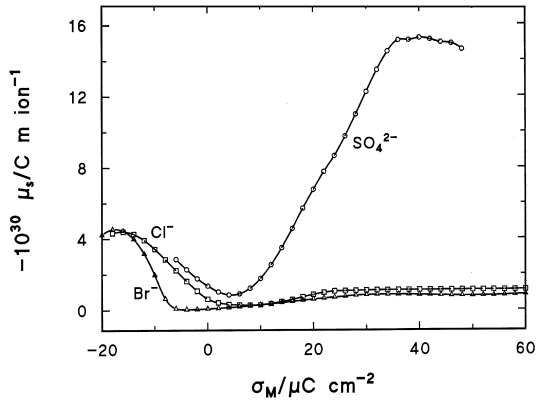


Fig. 4. Plots of the surface dipole moment of adsorbed anion at the Au(111) surface for (○) $SO_4^{2-}$; $Cl^-$ (□); $Br^-$ (△)

The absolute values of all dipole moments shown in Fig. 4 are much smaller than the value of −21 D (1 D = $3.336 \times 10^{-30}$ C m) for $SO_4^{2-}$, −8.69 D for $Cl^-$ and −9.36 D for $Br^-$, expected for a dipole formed by a charged sphere of charge $z$ and an ionic radius $r_i$ adsorbed on a perfect conductor (equal to the product $ze_0r$ [65]). The surface dipoles attain a minimum at small charge densities at the metal (near the zero charge). The minimum values of the surface dipole are −0.01 D for $Br^-$ −0.08 D for $Cl^-$ and −0.25 D for $SO_4^{2-}$. The numbers for the Au(111) surface may be compared to surface dipoles determined for the adsorption at the mercury electrode, which are equal to −0.95 D for $Br^-$, −1.25 D for $Cl^-$ and −2.85 D for $SO_4^{2-}$ [60, 65]. These results indicate that the dipole formed by adsorbed anion and its image charge in the metal is significantly screened by the solvent and the metal. The screening is apparently much stronger at the gold than at the mercury surface. Schmickler and Guidelli [64–66] described the screening as a combination of the spill-over of electrons from the metal and the polarization of the surface solvent molecules. The spill-over shortens the ion-image distance. The adsorbed ion polarizes the solvent molecules in its vicinity such that their dipoles assume an orientation opposite to the adsorbate dipole. The dipole on the solvent in turn depolarizes (screens) the dipole of the adsorbate. This model gives the calculated values of the surface dipoles which are in excellent agreement with experiment.

Figure 4 shows that for $\sigma_M > 10$ μC cm$^{-2}$, the dipole of adsorbed $SO_4^{2-}$ significantly increases with the charge on the metal and attains a constant value of −4.5 D at high charge densities. This result indicates that the screening effect diminishes with charge. Following Schmickler and Guidelli [64–66] we can explain this behavior in terms of the solvent displacement by adsorbed sulfate. At higher $SO_4^{2-}$ coverages the solvent molecules are squeezed out of the surface and hence the screening of the adsorbed dipole diminishes as well. For $Cl^-$ and $Br^-$, the surface dipole also increases with the charge, however, in contrast to sulfate, its absolute value remains small −0.3 D for $Cl^-$ and −0.25 D for $Br^-$ even at very high charge densities. The very small dipole moment for halides may be a result of charge redistribution due to the mixing of electronic states of the adsorbed anion with electronic states of the metal. In that case the adsorption of anion should affect the electronic structure of the metal.

### Electronic structure of the surface

The adsorbate induced changes of the electronic structure of the metal may be conveniently studied using second harmonic generation spectroscopy (SHG) [27–29, 67, 68] (see also electroreflectance studies of the metal electronic structure [35]). There are two major contributions to the measured SHG signal. The first comes from interactions of the elec-

tromagnetic fields of the incident photons with the free electrons in the metal and involves excitation of free electrons to a virtual state. The second arises from coupling of the optical fields of the incident photons with the interband transitions and has a resonant nature. It involves electronic transitions between two real electronic states. The lifetime of a virtual state is much shorter than the lifetime of a real excited electronic state. Consequently, the photons emitted by these two mechanisms are emitted at different times and consequently are phase shifted [69–71]. The mixing of the electronic states of the adsorbate with electronic states of the metal enhances the contribution of the interband transitions to the measured signal and hence changes the phase angle [29–37, 67]. The measurement of the phase angle provides a convenient means to study the adsorbate induced changes of the metal electronic structure. Accurate phase angle measurements require a proper selection of the reference state. An attractive method to measure the phase angle is the interference second harmonic generation spectroscopy (ISHG), introduced recently by Pettinger and Bilger [26]. In this technique, a quartz lamella is placed in the optical path of the incident photons and the phase of the SHG photons generated at the metal solution interface is measured with respect to the phase of the SHG photons generated by the quartz lamella. This technique has been applied to measure the potential and charge dependence of the phase angle at the Au(111) surface in the presence of specifically adsorbed anions, and the results are shown in Fig. 5.

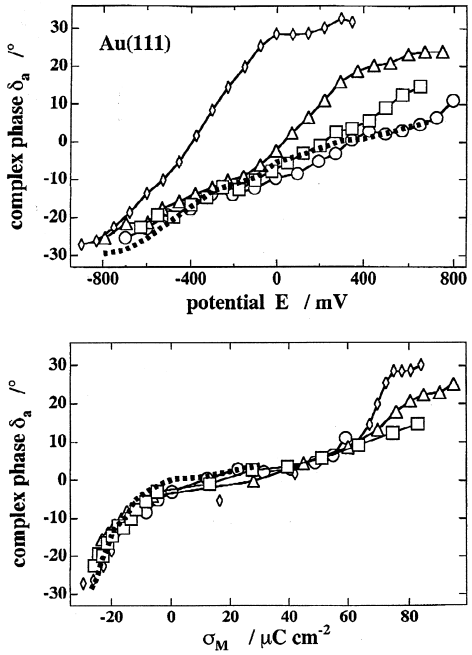


Fig. 5. Plot of the difference between the phase angle of the SHG photons generated at the Au(111) surface and in the quartz lamella in O.1 M $NaClO_4$ (■) and O.1 M $NaClO_4 + 10^{-3}$ M $Na_2SO_4$ (○), NaCl (□), NaBr (△), NaI (◇)

The top panel in Fig. 5 shows how the phase angle changes with the electrode potential for pure 0.1 M $NaClO_4$ and the sodium perchlorate solution with the addition of millimolar concentrations of the four anions, respectively. The phase angle displays quite a strong dependence on the electrode potential and the nature of the anion. These changes indicate that interband transitions contribute to the observed SHG signal. In the case of the Au electrode and the energy of the input photons 1.17 eV, the interband transitions involve the upper edge of d band located 2 eV below the Fermi level. The potential dependence of the phase angle apparently increases in the order $ClO_4^- \approx SO_4^{2-} < Cl^- < Br^- < I^-$, which corresponds to the sequence of the increasing adsorption strength. In our previous paper [23], we have interpreted such changes in terms of mixing of the electronic states of the adsorbate with the electronic states of the substrate, leading to a change of the electronic structure of the metal.

However, if the same phase angle data are plotted against the charge on the metal, bottom panel in Fig. 5, the dependence of the phase angle on the nature of the specifically adsorbed anion is too a large extent removed. For charge densities lower than 60 μC cm$^{-2}$, all phase angle data obey one common relationship. For charges higher than 60 μC cm$^{-2}$, the phase angle data corresponding to different anions diverge. This behavior correlates quite well with the fact that the anions form disordered (mobile) adlayers at $\sigma_M < 60$ μC cm$^{-2}$ and ordered (2D solid like) adlayers at higher charge densities. Apparently, for the mobile adlayer, the changes of the phase angle are due rather to the change of the field at the interface, than to the change of the electronic structure of the metal. In contrast, the electronic structure of the interface is changed when an ordered adlayer is formed. However, no apparent change of the electrosorption valency was observed at the potential of the order–disorder phase transition. Therefore, no extra charge is transferred to the interface when new electronic states are formed by the ordered adlayer. The SHG data do not indicate that the adsorption of anions involves mixing of the electronic states of the adsorbate and the substrate, and a charge transfer from the adsorbate to the metal. For adsorption of sulfate, this conclusion is supported by the core-level electron energy loss spectroscopy experiments by Wieckowski *et al.* [13, 14], which showed that sulfate adsorption at Au(111) does not affect the oxidation state of the sulfur atom. This discussion illustrates difficulties to determine the degree of charge transfer involved in the formation of the electrosorption bond and confirms once more that the best way to describe the polarity of the electro-

sorption bond is to use the surface dipole. Under no circumstances should the electrosorption valency be discussed in terms of a partial charge transfer if there are no independent spectroscopic data to support this argument.

### Structure of the surface and the adlayer

It is now well established, by various structure-sensitive techniques that, in contact with an electrolyte solution, the Au(111) surface is reconstructed if it is negatively charged, and the reconstruction is lifted when the metal is charged positively [4–32, 45, 49]. This behavior is consistent with electronic theories which explain the reconstruction of Au surfaces in vacuum in terms of a compressive stress of s–p electrons balanced by a repulsive interaction of the filled d-shells [72–76]. Negative charging of the metal surface increases the density of s–p electrons and hence increases the compressive stress. This stress forces surface atoms to form a more tightly packed reconstructed structure. In contrast, positive charging of the surface decreases the density of s–p electrons and hence reduces the compressive stress. Therefore, the surface atoms relax into the more open $(1 \times 1)$ structure. However, it is also well known that the stability of the reconstructed surface is strongly affected by the ionic adsorption [31, 49]. Alternatively, lifting of the reconstruction may be explained by the different adsorption energies of anions at the reconstructed and unreconstructed surfaces [49].

What are the charge densities and the surface concentrations of the adsorbed anion at which the reconstruction is lifted? To answer this question, one has to combine the knowledge of surface coverages and charge densities derived from the thermodynamic studies with independent structural measurements. This problem illustrates the complementarity of the macroscopic (thermodynamic) and structural (microscopic) studies. Recently, Ocko *et al.* [32] applied surface X-ray scattering and chronocoulometric techniques to study lifting the reconstruction of the Au(111) electrode in the presence of adsorbed Br ions. Figure 6 summarizes the main results of these experiments. The three panels show the potential dependence of the integrated intensity of the surface truncation rod corresponding to the X-ray scattering by the reconstructed surface (top panel); the charge density at the metal (middle panel) and surface concentration of adsorbed Br (bottom panel). Below $E = -0.15$ V, the surface is reconstructed. This region corresponds to charge densities lower than $-8\ \mu C\ cm^2$ and surface concentration of $Br^-$ lower than $8 \times 10^{13}$ ions $cm^2$. This latter value corresponds to about 10% of the saturated bromide surface concentration of $8 \times 10^{14}$ ions $cm^2$. At $E = -0.15$ V, the X-ray intensity begins to drop and by $E = -0.095$ V it has only 20% of its original value. In this range, the charge density has increased to $+20\ \mu C\ cm^{-2}$ and

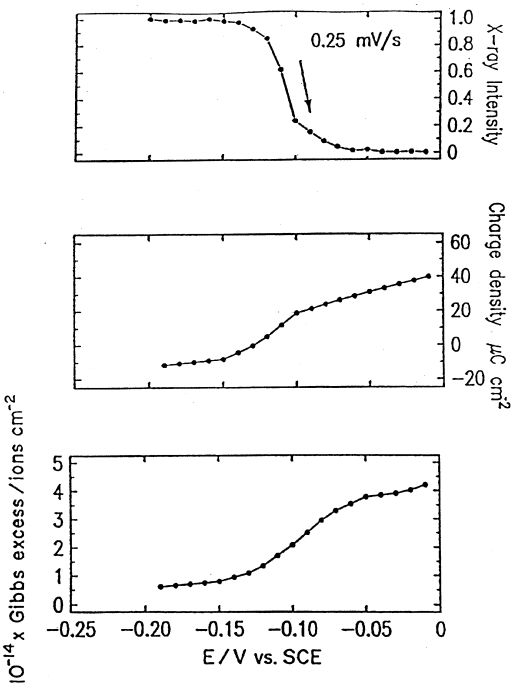


Fig. 6. Potential dependence of: (top panel) integrated scattered X-ray intensity in the vicinity of (–0.044, 1.022, 0.2), (middle panel) charge density at the metal surface, (bottom panel) surface concentration of adsorbed $Br^-$ for Au(111) electrode in 0.1 M $KClO_4$ + 0.01 M KBr (adapted from Ref. [32])

surface concentration to $2 \times 10^{14}$ ions $cm^2$. This latter value corresponds to a quarter of the saturated bromide surface concentration. Apparently, the lifting of the reconstruction spans a potential range of about 60 mV, where the surface charge changes from $-10$ to $20\ \mu C\ cm^{-2}$ and bromide coverage increases from 10% to 25% of its saturation value. Since the changes of charge are paralleled by a significant increase of the surface coverage by adsorbed bromide, it is difficult to establish whether the reconstruction is lifted by surface charge or by bromide adsorption. The above studies demonstrate that the structure of the Au(111) surface changes with potential, charge and coverage. For negative charge densities and low surface coverages, thermodynamic data correspond to adsorption at the reconstructed $(p \times \sqrt{3})$ surface and for positive charges and high coverages the data represent adsorption at the unreconstructed $(1 \times 1)$ substrate.

It is now well established that adlayers of adsorbed anions are disordered (mobile) up to coverages of about 94% of the saturated value [77]. At higher coverages, formation of ordered two dimensional structures is observed. These ordered adlayers are formed at the unreconstructed $(1 \times 1)$ gold surface. STM studies revealed that sulfate forms a commensurate $(\sqrt{3} \times \sqrt{7})$ structure at the positive end of potentials, near the onset of gold

oxidation [4, 15–17]. Similar structures were observed on Pt(111) [78, 79] and Ru(111) [80] electrodes. The model of this structure and the interpretation of STM images evolved with time and these changes illustrate how the availability of precise surface coverage data, derived from chronocoulometric experiments, may assist in the interpretation of STM images. The first STM images for the ordered sulfate adlayer, reported by Magnussen *et al.* [15], were interpreted as images of hydrogen-bound bisulfate corresponding to the total coverage 0.4 ML [15] (where 1 ML coverage corresponds to the surface concentration of gold atoms at an ideal Au(111) surface $1.39 \times 10^{15}$ atoms $cm^{-2}$). However, chronocoulometric and radiochemical studies by Shi *et al.* [5] demonstrated later, that the adsorbed species is sulfate not bisulfate and that the limiting sulfate coverage amounts to only 0.2 ML. Weaver *et al.* [5, 16, 17] performed additional STM and FTIR studies of this system and, to reconcile the results of chronocoulometric and STM measurements, proposed a model in which hydronium ions are incorporated into the $(\sqrt{3} \times \sqrt{7})$ network. This model was further developed by Itaya *et al.* [80] who incorporated hydrogen bonded water chains into the $(\sqrt{3} \times \sqrt{7})$ network of adsorbed sulfate. The Itaya model is shown in Fig. 7. The coverage of sulfate ions corresponds to 0.2 ML, consistent with the results of chronocoulometric and radiochemical measurements. The water chains are inserted along the $\sqrt{3}$ direction between the neighboring sulfate atoms. This model resembles the hexagonal ice water structure and is a likely representation of the actual structure of the adlayer.

The formation of ordered adlayers by halides at gold electrodes was recently reviewed by Ocko and Wandlowski [77] and we will summarize here the main points only. Early STM studies of the adlayers formed by $Br^-$ [30] and $I^-$ [40–42] suggested that halides form commensurate structures. However, more precise surface X-ray scattering experiments revealed that the overlayers are incommensurate. All three halides form uniaxial-incommensurate $c(p \times \sqrt{3})$ structures, which in the case of iodide is transformed into the rotated-hexagonal structure, at higher coverages. The two structures are shown in Fig. 8. These structures are electrocompressible and the spacing between the adsorbed species continuously decreases with the electrode potential. Consequently, the coverage of the electrode surface progressively increases with potential. For bromide, surface concentration determined from the dimensions of the 2D unit cell of the adlayer are compared to the Gibbs excesses determined from independent chronocoulometric measurements in Fig. 9. The coverages determined from diffraction and that obtained from the thermodynamic analysis of the charge density data agree within a few percent. The slope of the coverage-plots gives the electrocompressibility of the adlayer. The measured electrocompressibilities $\partial\Gamma/\partial E$ ($10^{14}$ ions $cm^{-2}$ $V^{-1}$) are $2.41 \pm 0.15$; $2.95 \pm 0.07$ and $1.98 \pm 0.02$ for $Cl^-$, $Br^-$ and $I^-$, respectively [21, 77]. Despite the different sizes of

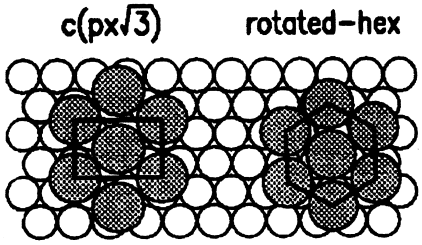


Fig. 8. Atomic models of halide structures at Au(111) surface (adapted from Ref. [77])

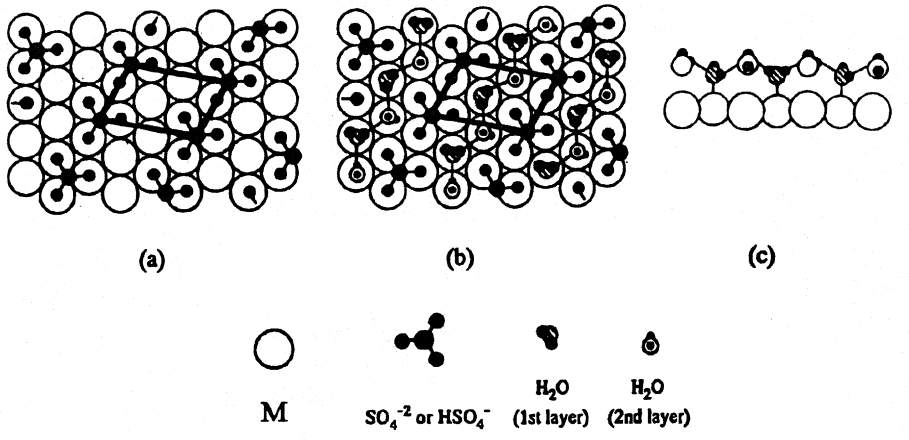


Fig. 7. The Itaya model of the $(\sqrt{3} \times \sqrt{7})$ structure of ordered adlayer formed by co-adsorption of sulfate and water molecules: (a) Sulfate on the 3-fold site; (b) co-adsorption of sulfate and hydrogen-bonded water chains; (c) side view of the hydrogen-bonded water chain along the $\sqrt{3}$ direction (taken from Ref. [80])

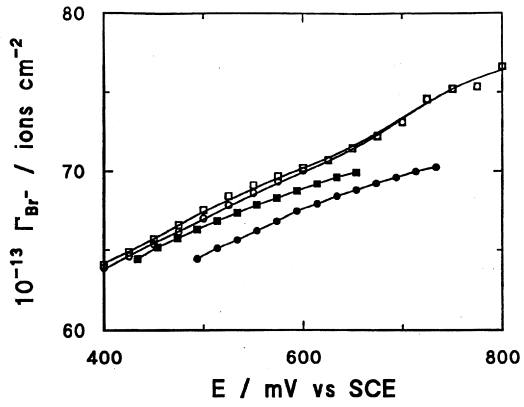


Fig. 9. Comparison of Gibbs excesses for $Br^-$ adsorption at the Au(111) electrode, determined from chronocoulometric experiments in 0.1 M $KClO_4 + 10^{-3}$ M KBr (○) and 0.1 M $KClO_4 + 10^{-2}$ M KBr (□) solutions, with surface concentrations, calculated from the dimensions of the unit cell of the c(p × $\sqrt{3}$) Br adlayer in 0.1 M $HClO_4 + 10^{-3}$ M KBr (●) and 0.1 M $HClO_4 + 10^{-2}$ M KBr (■)

the three halides and the potential range where these ordered adlayers are formed, they display very similar electrocompressibilities.

These facts provide important information about the nature of the halide–gold bond and about the character of the lateral interactions between the adsorbed adions. The incommensurate character of the overlayer structure indicates that the halide–gold bond does not have a well defined directionality and cannot be described in terms of singular values of bond length, bond angle and coordination number. The similar electro-compressibility of the ordered overlayers indicates that the repulsive interactions are similar for each of the three halide adions. Ocko and Wandlowski pointed out that the repulsive interactions between halide adions are likely to have a dipole–dipole character [77]. This conclusion is consistent with the surface dipole values shown in Fig. 4. At potentials where the ordered adlayers are formed, the surface dipoles for chloride and bromide are equal to −0.3 D and −0.25 D, respectively and hence are of comparable magnitude. Therefore, this is once more a case where quantities derived from macroscopic experiments provide information needed for the interpretation of structural data.

## Model of the inner layer

Many models were developed to describe the structure of the metal solution interface in the presence of the specific adsorption of anions. These efforts were reviewed recently by Schmickler [61, 62, 81]. Most of the data obtained for mercury and for solid electrodes were analyzed in terms of the Grahame–Parsons model of the inner part of the double layer [52, 58]. The model treats the inner layer as a dielectric continuum, assumes a total separation of charge at the interface, and a specific location for the adsorbed species (inner Helmholtz plane at a distance $x_1$ from the metal surface). Despite inadequacies of this model, which were discussed by Schmickler [61, 81], we will employ it below to describe ionic adsorption at the Au(111) surface. This model has been used to describe large numbers of adsorption data and hence our analysis could be used at least for comparative purposes.

The capacity of the inner layer $C^i$ may be calculated from the overall electrode capacity $C$ determined by differentiation of the charge density curves and using the theory of the diffuse layer, with the help of the formula [82]:

$$(C^i)^{-1} = (C)^{-1} - (1 - F(\partial\Gamma/(\sigma_M)_\mu)(C^d)^{-1} \quad (11)$$

where $C^d$ is the capacity of the diffuse layer and $(\partial\Gamma/\partial\sigma_M)_\mu$ is the Esin–Markov coefficient. Figure 10 shows the inner layer capacities calculated with the help of equation (11). The inner layer capacities are to a good approximation independent of the bulk concentration of the anion. They display a large peak at charge densities close to zero which increases by moving from $SO_4^{2-}$ to $Br^-$. This trend corresponds to the order of increasing adsorption strength.

The inner layer capacity is a function of two variables, charge on the metal and the amount of adsorbed anion. It may therefore be expressed in terms of two components, capacity of the inner layer at a constant charge ($_\Gamma C$) and capacity of the inner layer at a constant amount adsorbed ($_\sigma C$), as described by the formula [82]:

$$(C^i)^{-1} = (_\sigma C)^{-1} - F(\partial\Gamma/\partial\sigma_M)_\mu(_\Gamma C)^{-1} \quad (12)$$

The capacity $_\Gamma C$ may be determined from the slope of the plot of the potential drop across the inner

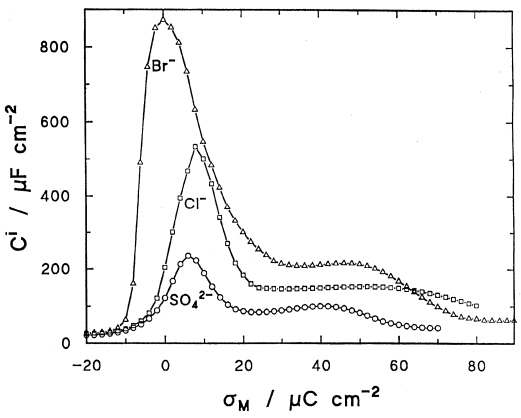


Fig. 10. Inner layer capacities determined for the Au(111) electrode in 0.1 M $HClO_4 + 10^{-3}$ M $K_2SO_4$ (○) 0.1 M $KClO_4 + 10^{-3}$ M potassium salt of $Cl^-$ (□) and $Br^-$ (△)

layer, $\Delta\phi^{M-2} = E - E_{pzc} - \phi_2$, vs. the charge of adsorbed anion, $z_i F \Gamma_i$, at a constant $\sigma_M$ ($\phi_2$ is the outer Helmholtz plane potential). The values of ${}_\Gamma C$ and equation (12) may then be used to calculate the capacity at a constant amount adsorbed ${}_\sigma C$. The capacities at constant charge and constant amount adsorbed may be considered as integral capacities described by [59]:

$$ {}_\Gamma C = \varepsilon/(x_2 - x_1) \tag{13}$$

and

$$ {}_\sigma C = \varepsilon/x_2 \tag{14}$$

Fig. 11(a) and (b) show the components of the inner-layer capacity at constant charge and constant amount adsorbed, respectively. For charge densities larger than 10 μC cm$^{-2}$, the two components of the inner layer capacity increase in the order $SO_4^{2-} < Br^- < Cl^-$, which correlates well with the sequence of decreasing anion size. This trend is not preserved for small charges, where capacities ${}_\Gamma C$ and ${}_\sigma C$ display a maximum. The interpretation of ${}_\Gamma C$ curves is difficult, since they may be affected by both the change of the permittivity and the position of the inner Helmholtz plane $x_1$. The interpretation of ${}_\sigma C$ curves is easier, particularly if one assumes that the thickness of the inner layer $x_2$ does not change with charge. The shape of ${}_\sigma C$ displays how its permittivity changes with the charge on the metal. The changes of the permittivity may be correlated with the orientation of water dipoles at the electrode surface. Due to the dielectric saturation, the permittivity is expected to be low at either very negative or very positive potentials and to display a maximum at small charge density where the solvent molecules reorient and disorientation of water dipoles is at maximum. The changes of the inner layer capacity at the constant amount adsorbed should correlate well with the ability of the solvent molecules to screen the surface dipole formed by adsorbed anion and discussed in the preceding section.

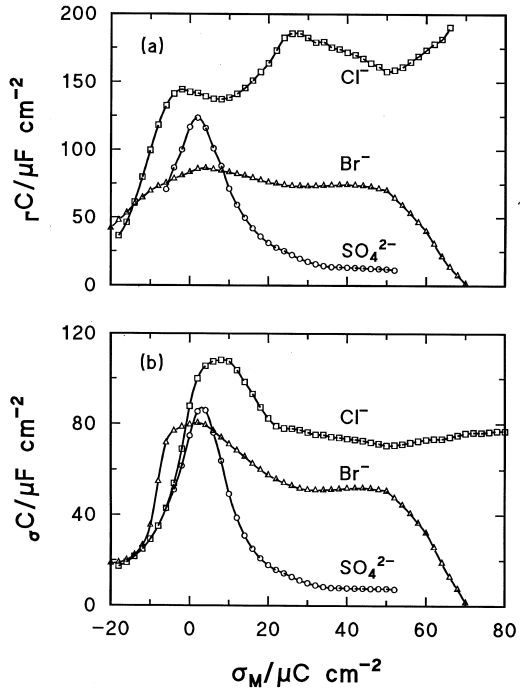


Fig. 11. The components of the inner layer capacity at a constant charge (top panel) and constant amount adsorbed (bottom panel) for the Au(111) electrode in (○) $SO_4^{2-}$, (□) $Cl^-$ and (△) $Br^-$ solutions

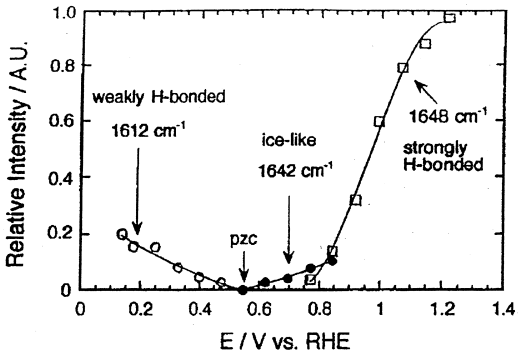


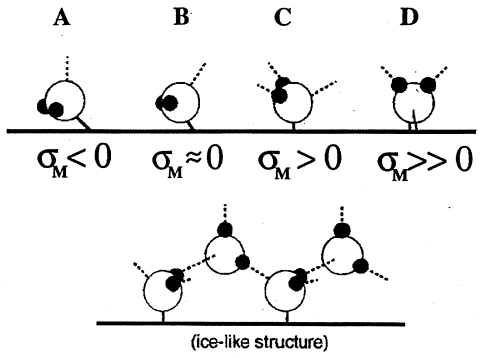


Fig. 12. Plot of the integrated intensities of δHOH bands as a function of applied potential for a highly ordered Au(111) electrode in 0.5 M $HClO_4$ solution (adapted from Ref. [88])

The surface charge or adsorbate induced solvent reorientation has frequently been invoked in the modeling of the electrical double layer. However, only very recently X-ray diffraction and infrared spectroscopy have been employed to probe the structure of water at electrode surfaces. The X-ray reflectivity measurements by Toney *et al.* [83, 84] indicate that surface water has much higher density at either positively or negatively charged surface and that the density goes through a minimum around the zero charge value. Further details concerning the orientation of surface water molecules are provided by surface enhanced infrared absorption spectroscopy experiments by Ataka *et al.* [85]. For Au

electrode in perchloric acid solution, the shape of IR spectra for surface water molecules evolves as function of the electrode potential. These changes can be assigned to different orientations of surface water molecules. Figure 12, taken from Ref. [85], plots intensity of the $\delta$HOH scissor mode of a water molecule (1650–1610 $cm^{-1}$) as a function of the electrode potential. At the negatively charged surface the band is red shifted and its spectral features are consistent with the surface orientation of water molecules shown by model A. Around the pzc surface water molecules assume an orientation in which the dipole moment is parallel to the surface. At moderately positive charges the ice-liked structure is postulated. At the most positive potentials where perchlorate anions adsorb, the surface water molecules further reorient to orientation D. These results are in an overall qualitative agreement with the solvent reorientation models. They also provide the first direct evidence that specific adsorption of an anion affects the surface orientation of water molecules.

There are significant differences between the shape of $_{\sigma}C$ curves determined for sulfate and for the two halides. The curve for sulfate has a symmetric bell shape in good qualitative agreement with the predictions of solvent reorientation theories [61, 62, 81]. In contrast, for halides the capacities at constant amount adsorbed are quite asymmetric and display a second broad maximum at more positive charge densities. These differences suggest that specifically adsorbed anions may significantly affect the orientation of adsorbed water molecules. These differences offer an interesting opportunity to test the validity of the Grahame–Parsons model of the inner layer. One may hope, that from future spectroscopic studies, such as that carried out by Ataka *et al*., we will learn more about the influence of specifically adsorbed anions on the surface orientation of water. The capacities at a constant amount adsorbed may be used as a guide for such studies. The results of these experiments may then prove or disprove the validity of classical models of the inner part of the double layer.

## CONCLUSIONS AND OUTLOOK

We have presented a unified description of ionic adsorption at gold electrodes in which a molecular level interpretation is given to the thermodynamic parameters characterizing energetics of the adsorption equilibrium. This approach requires a concerted use of thermodynamic and spectroscopic, imaging and diffraction techniques. The macroscopic and microscopic methods are complementary. The knowledge derived from thermodynamic studies provide a framework which links together molecular level information obtained from various seemingly disjoint microscopic experiments. The knowledge of thermodynamic parameters is needed for the design of the microscopic experiments and the interpretation of their results. In turn, the spectroscopic, molecular imaging and diffraction data provide the needed atomic level description of the phenomena observed so far at the macroscopic level. This microscopic information is essential to verify the validity of various theories and models of the electrified interface.

Due to the technological and methodological developments, we have achieved an unprecedented level of understanding of ionic adsorption at metal electrodes. However, many issues remained to be resolved. The topic which perhaps deserves the most urgent attention is the structure of water at electrode surfaces. Recent work by Ataka *et al*. [85] demonstrated that FTIR experiments may provide direct information about orientation of solvent molecules at the electrode surface. In addition, the vibrational sum–frequency spectroscopy has a unique potential to probe solvent molecules at surfaces and this technique should be employed in the near future to study charge or adsorbate induced solvent reorientation phenomena. The unified macroscopic and microscopic picture of ionic adsorption at metal electrodes is presently available for the Au(111) electrode and for four anions only. Thermodynamic and atomistic studies should be extended to included information about the surface properties of other anions, specifically oxy-anions. The recent studies by Silva [86] show how much we can learn by pursuing this direction. The studies of ionic adsorption should be extended onto other crystallographic orientations of gold. The formation of ordered adlayers indicates that the metal surface no longer may be treated as a conductive wall and that the electrosorption bond formation has an interesting coordination chemistry. Finally, investigations of ionic adsorption at solid electrodes should be extended to metals other than gold. The thermodynamic and STM studies by Guidelli and Foresti [63, 87], and X-ray diffraction studies by Ocko *et al*. [77], have already provided a very advanced picture of ionic adsorption at silver single crystal electrodes. Finally, thermodynamic methods have been recently applied to study ionic adsorption at Pt single crystal electrodes by Savich *et al*. [88]. This work opened a new opportunity to conduct concerted macroscopic and microscopic investigations of ionic adsorption at d metals.

## ACKNOWLEDGEMENTS

This work was supported by a grant from the Natural Sciences and Engineering Research Council of Canada. J. L. acknowledges helpful discussions with O. M. Magnussen, J. X. Wang and B. M. Ocko and thanks Alexander von Humboldt-Stiftung for the Research Award.

## REFERENCES


1. R. Parsons, *Chem. Rev*. **90,** 813 (1990).
2. A. Hamelin, in *Modern Aspects of Electrochemistry*, Vol. 9, eds. B. E. Conway and J. O'M. Bockris, Plenum Press, New York, 1985, p. 1.
3. J. Lipkowski, *Adsorption of Molecules at Metal Electrodes*, eds. J. Lipkowski and P. N. Ross, VCH, New York, 1992, p. 171.
4. X. Gao, G. J. Edens and M. Weaver, *J. Electroanal. Chem*. **376,** 21 (1994).
5. Z. Shi, J. Lipkowski, M. Gamboa, P. Zelenay and A. Wieckowski, *J. Electroanal. Chem*. **366,** 317 (1994).
6. Z. Shi, J. Lipkowski, S. Mirwald and B. Pettinger, *J. Electroanal. Chem*. **396,** 115 (1995).
7. S. Mirwald, B. Pettinger and J. Lipkowski, *Surf. Sci*. **335,** 264 (1995).
8. D. A. Scherson and D. M. Kolb, *J. Electroanal. Chem*. **176,** 35 (1984).
9. H. Angerstein-Kozlowska, B. E. Conway, A. Hamelin and L. Stoicovicu, *Electrochim. Acta* **31,** 1052 (1986).
10. H. Angerstein-Kozlowska, B. E. Conway, A. Hamelin and L. Stoicovicu, *J. Electroanal. Chem*. **228,** 429 (1987).
11. M. S. Zei, D. Scherson, G. Lehmpfuhl and D. M. Kolb, *J. Electroanal. Chem*. **229,** 99 (1987).
12. M. S. Zei, G. Qiao, G. Lehmpfuhl and D. M. Kolb, *Ber. Bunsenges. Phys. Chem*. **91,** 349 (1987).
13. P. Mrozek, M. Han, Y.-E. Sung and A. Wieckowski, *Surf. Sci*. **319,** 21 (1994).
14. S. Thomas, Y.-E. Sung and A. Wieckowski, Solid–liquid electrochemical interfaces, ed. G. Jerkiewicz, M. P. Soriaga, K. V. Saki and A. Wieckowski, ACS Symp. Ser. 656, 1997, p. 126. Washington, DC.
15. O. M. Magnussen, J. Hageboeck, J. Hotlos and R. J. Behm, *Faraday Discuss. Chem. Soc*. **94,** 329 (1992).
16. G. J. Eden, X. Gao and M. J. Weaver, *J. Electroanal. Chem*. **375,** 357 (1994).
17. G. J. Eden, *Interface* **3,** 45 (1994).
18. H. Uchida, N. Ikeda and M. Watanabe, *J. Electroanal. Chem*. **424,** 5 (1997).
19. Z. Shi and J. Lipkowski, *J. Electroanal. Chem*. **403,** 225 (1996).
20. A. Kolics, A. E. Thomas and A. Wieckowski, *J. Chem. Soc., Faraday Trans*. **92,** 3727 (1996).
21. O. M. Magnussen, B. M. Ocko, J. Wang and R. R. Adzic, *Phys. Rev*. **B 51,** 5510 (1995).
22. H.-W. Lei, H. Uchida and M. Watanabe, *Langmuir* **13,** 3523 (1997).
23. Z. Shi, J. Lipkowski, S. Mirwald and B. Pettinger, *J. Chem. Soc. Faraday Trans*. **92,** 3737 (1996).
24. D. M. Kolb, W. N. Hansen, D. L. Rath and R. Wille, *Ber. Bunsenges. Phys. Chem*. **87,** 1108 (1987).
25. D. M. Kolb, *Z. Phys. Chem. Neue Folge* **154,** 179 (1983).
26. B. Pettinger and C. Bilger, Phys. Rev. Lett. 1997, in press.
27. A. Friedrich, B. Pettinger, D. M. Kolb, G. Luebke, R. Steinchoff and G. Marowsky, *Chem. Phys. Lett*. **163,** 123 (1989).
28. B. Pettinger, J. Lipkowski, S. Mirwald and A. Friedrich, *J. Electroanal. Chem*. **329,** 289 (1992).
29. B. Pettinger, J. Lipkowski and S. Mirwald, *Electrochim. Acta* **40,** 133 (1995).
30. N. J. Tao and S. M. Lindsay, *J. Phys. Chem*. **96,** 5213 (1992).
31. J. Wang, B. M. Ocko, A. J. Devenport and H. S. Isaacs, *Phys. Rev*. **B34,** 10321 (1992).
32. B. M. Ocko, O. M. Magnussen, J. Wang, R. R. Adzic, Z. Shi and J. Lipkowski, *J. Electroanal. Chem*. **376,** 35 (1994).
33. O. M. Magnussen, J. X. Wang, R. R. Adzic and B. M. Ocko, *J. Phys. Chem*. **100,** 5500 (1996).
34. R. R. Adzic, E. Yeager and B. D. Cahan, *J. Electroanal. Chem*. **85,** 267 (1977).
35. D. M. Kolb and C. Franke, *Appl. Phys*. **A 49,** 379 (1982).
36. M. R. Deakin, T. T. Li and O. R. Melroy, *J. Electroanal. Chem*. **243,** 343 (1988).
37. N. Batina, T. Yamada and K. Itaya, *Langmuir* **11,** 4568 (1995).
38. B. G. Bravo, S. L. Michelhaugh, M. P. Soriaga, I. Villegas, D. W. Suggs and J. L. Stickney, *J. Phys. Chem*. **95,** 5245 (1991).
39. X. Gao and M. J. Weaver, *J. Am. Chem. Soc*. **114,** 8544 (1992).
40. H. Matsumoto, J. Inukai and M. Ito, *J. Electroanal. Chem*. **379,** 223 (1994).
41. X. Gao, G. J. Edens, F. C. Liu, A. Hamelin and M. J. Weaver, *J. Phys. Chem*., **98**, 8086 (1994).
42. W. Haiss, J. K. Sass, X. Gao and M. J. Weaver, *Surf. Sci*. **274,** L593 (1992).
43. T. L. Yamada, N. Batina and K. Itaya, *Surf. Sci*. **335,** 204 (1995).
44. T. L. Yamada, N. Batina and K. Itaya, *J. Phys. Chem*. **99,** 8817 (1995).
45. B. M. Ocko, G. M. Watson and J. Wang, *J. Phys. Chem*. **98,** 897 (1994).
46. J. Richer and J. Lipkowski, *J. Electrochem. Soc*. **133,** 121 (1986).
47. A. Chen, Z. Shi, D. Bizzotto, J. Lipkowski, C. Bilger and B. Pettinger, Langmuir, submitted for publication.
48. Z. Shi, S. Wu and J. Lipkowski, *Electrochim. Acta* **40,** 9 (1995).
49. D. M. Kolb, *Prog. Surf. Sci*. **51,** 109 (1996).
50. West R. C. (Ed.), *Handbook of Chemistry and Physics*, CRC Press, Palm Beach, FL, 1978.
51. L. Blum and D. A. Huckaby, *J. Electroanal. Chem*. **315,** 255 (1991).
52. D. C. Grahame, *J. Am. Chem. Soc*. **80,** 4201 (1958).
53. R. Parsons and S. Trasatti, *J. Electroanal. Chem*. **205,** 359 (1986).
54. L.-W. Leung, T. W. Gregg and D. W. Goodman, *Langmuir* **7,** 3205 (1991).
55. N. Markovic and P. N. Ross, *Langmuir* **9,** 580 (1993).
56. P. N. Ross and N. Markovic, *Langmuir* **10,** 976 (1994).
57. L.-W. Leung and D. W. Goodman, *Langmuir* **10,** 978 (1994).
58. D. C. Grahame and R. Parsons, *J. Am. Chem. Soc*. **83,** 1291 (1961).
59. K. Bange, R. Parsons, J. K. Sass and B. Straehler, *J. Electroanal. Chem*. **229,** 87 (1987).
60. R. Parsons, *Bull. Electrochem*. **6,** 566 (1990).
61. W. Schmickler, in *Structure of Electrified Interfaces*, eds. J. Lipkowski and P. N. Ross, VCH, New York, 1993, p. 201.
62. W. Schmickler, *Interfacial Electrochemistry*. Oxford University Press, London, 1996, Ch. 18.
63. M. L. Foresti, G. Aloisi, M. Innocenti, H. Kobayashi and R. Guidelli, *Surf. Sci*. **335,** 241 (1995).
64. W. Schmickler and R. Guidelli, *J. Electroanal. Chem*. **235,** 387 (1987).
65. W. Schmickler, *J. Electroanal. Chem*. **249,** 25 (1988).
66. W. Schmickler, *Ber. Bunsenges. Phys. Chem*. **92,** 1203 (1988).
67. B. Pettinger, S. Mirwald and J. Lipkowski, *Surf. Sci*. **335,** 264 (1995).
68. R. M. Corn and D. H. Higgins, *Chem. Rev*. **94,** 107 (1994).
69. D. A. Koos, V. L. Shannon and G. L. Richmond, *J. Phys. Chem*. **94,** 2091 (1990).
70. R. Georgiadis and G. L. Richmond, *J. Phys. Chem*. **95,** 2895 (1991).
71. E. K. Wong and G. L. Richmond, *J. Phys. Chem*. **99,** 5500 (1993).

72. D. Tomanek and K. H. Bennemann, *Surf. Sci.* **163,** 503 (1985).
73. V. Heine and L. D. Marks, *Surf. Sci.* **165,** 65 (1986).
74. C. L. Fu and K. M. Ho, *Phys. Rev. Lett.* **63,** 1617 (1989).
75. A. A. Kornyshev and I. Vifan, *Electrochim. Acta* **40,** 109 (1995).
76. K. P. Bohnen and K. M. Ho, *Electrochim. Acta* **40,** 129 (1995).
77. B. M. Ocko and Th. Wandlowski, ed. P. C. Andricacos, S. G. Corcoran, Y. L. Deplancke, T. P. Moffat and P. S. Searsan, Electrochemical Synthesis and Modifications of Materials, *Mat. Res. Soc. Symp. Proc.,* **455**, 55–68 (1997).
78. A. M. Funtikov, U. Linke, U. Stimming and R. Vogel, *Surf. Sci.* **324,** L343 (1995).
79. A. M. Funtikov, U. Stimming and R. Vogel, *J. Electroanal. Chem.* **428,** 147 (1997).
80. L.-J. Wan, S.-L. Yau and K. Itaya, *J. Phys. Chem.* **99,** 9507 (1995).
81. W. Schmickler, *Chem. Rev.* **96,** 3177 (1996).
82. R. Parsons, *Trans. Faraday Soc.* **55,** 999 (1959).
83. M. F. Toney, J. N. Howard, J. Richer, G. L. Borges, J. G. Gordon, O. R. Melroy, D. G. Wiesler, D. Yee and L. B. Sorensen, *Nature* **368,** 444 (1994).
84. M. F. Toney, J. N. Howard, J. Richer, G. L. Borges, J. G. Gordon, O. R. Melroy, D. G. Wiesler, D. Yee and L. B. Sorensen, *Surf. Sci.* **335,** 326 (1994).
85. K. Ataka, T. Yotsuyanagi and M. Osawa, *J. Phys. Chem* **100,** 10664 (1996).
86. F. Silva, Fischer Symp., this issue.
87. M. L. Foresti, M. Innocenti, H. Kobayashi, G. Pezzatini and R. Guidelli, *J. Chem. Soc. Faraday Trans.* **92,** 3747 (1996).
88. W. Savich, S.-G. Sun, J. Lipkowski and A. Wieckowski, *J. Electroanal. Chem.* **388,** 233 (1995).